Catalysis Science & Technology

PAPER

View Article Online
View Journal

Cite this: DOI: 10.1039/c5cy01542a

Fabrication of a Ti-supported $NiCo_2O_4$ nanosheet array and its superior catalytic performance in the hydrolysis of ammonia borane for hydrogen generation†

Jinyun Liao, Hao Li,* Xibin Zhang, Kejun Feng and Yanling Yao

Received 12th September 2015,
Accepted 25th December 2015

DOI: 10.1039/c5cy01542a

www.rsc.org/catalysis

The development of low-cost nanocatalysts with high activity, high stability and good reusability towards the hydrolysis of chemical hydrides for hydrogen generation is of great importance and significance in the field of hydrogen energy. In this work, a Ti-supported $NiCo_2O_4$ thin film nanosheet array ($NiCo_2O_4$/Ti) is fabricated by a facile method, and its catalytic performance in the hydrolysis of ammonia borane for hydrogen production is investigated. It is found that the turnover frequency (TOF) of $NiCo_2O_4$/Ti can reach 50.1 mol H_2 min^{-1} (mol catalyst)$^{-1}$, which is the highest TOF value reported for noble-metal-free catalysts towards the hydrolysis of ammonia borane. The apparent activation energy of ammonia borane hydrolysis in the presence of the $NiCo_2O_4$/Ti catalyst is as low as *ca.* 17.5 kJ mol^{-1}. More importantly, the $NiCo_2O_4$/Ti catalyst can retain *ca.* 90% of its original catalytic activity after 10 cycles, exhibiting much improved durability and reusability in contrast to many nanocatalysts recently reported in the literature. Its high catalytic activity and low-cost, together with its good durability and reusability, enable $NiCo_2O_4$/Ti to be a strong catalyst candidate for the hydrolysis of ammonia borane for hydrogen production in the practical applications.

Introduction

The consumption of energy in the world keeps on rising and the present energy system based on fossil fuels produces a large amount of pollutants, including carbon dioxide, which is regarded as a major cause of the "greenhouse effect". There is no doubt that seeking sustainable, environment-friendly and cost-effective energy sources is one of the most important tasks in the 21st century. Hydrogen is considered to be an ideal fuel for heating, mechanical power, transportation, as well as electricity generation, on account of its high energy density (142 MJ kg^{-1}), zero emissions and sufficient source.[1,2] Over the past few decades, a number of techniques have been developed to generate and store hydrogen. Particularly, the production of hydrogen by catalytic hydrolysis of chemical hydrides, such as $NaBH_4$, N_2H_4 and NH_3BH_3 (ammonia borane, AB), has received much attention in view of its high efficiency, convenience and safety.[3–6] For example, three moles of hydrogen will be produced when one mole of AB reacts with two moles of water in the presence of an appropriate catalyst *via* the following reaction equation:

$$H_3NBH_3(aq) + 2H_2O(l) \rightarrow NH_4^+(aq) + BO_2^-(aq) + 3H_2(g) \quad (1)$$

In the above hydrolytic reaction, the catalyst plays a crucial role in determining the efficiency and rate of hydrogen generation. Over the past decade, it has been well demonstrated that noble-metal-based catalysts, such as Pt,[5,7] Ru,[8–10] Pd,[11] CoPd,[12] CuPd,[13] NiPd (ref. 14) and PdPt,[15] exhibit relatively high catalytic activity in AB hydrolysis. However, their large-scale applications were restricted by high costs and scarcity. In contrast, noble-metal-free catalysts are more attractive due to their greater potential in practical applications. In recent years, many efforts have been devoted to the development of low-cost catalysts for AB hydrolysis and numerous inexpensive nanocatalysts have been reported, including Co,[16–18] Ni,[19] CoB,[20] CoP,[21] and Co–Mo–B–P.[22] However, most of them suffer from difficult isolation from the reaction solutions, lower activity in contrast to noble metal catalysts, and poor stability or reusability. So, the development of cost-effective, highly active and stable catalysts for AB hydrolysis is highly desirable, which is still a big challenge. On the other hand, most of these low-cost nanocatalysts for AB hydrolysis reported in the literature are Co,

Department of Chemical Engineering, Huizhou University, Huizhou, 516007, China. E-mail: lihao180@126.com; Fax: +86 752 2527229; Tel: +86 752 2527229

† Electronic supplementary information (ESI) available: Digital camera photos and SEM images. See DOI: 10.1039/c5cy01542a

Ni or their alloys. Therefore, it is of great importance and significance to develop other types of catalysts rather than metals or alloys.

In this work, a Ti-supported $NiCo_2O_4$ nanosheet array was fabricated by a facile process and its catalytic performance in the hydrolysis of AB was investigated. It should be mentioned that the $NiCo_2O_4$ nanostructures for high-performance supercapacitors have been intensively reported over the past few years;[23–25] however, their applications as catalysts in heterogeneous catalysis have been seldom dealt with. As far as we know, this is the first investigation on $NiCo_2O_4$ nanostructures as a catalyst towards AB hydrolysis for hydrogen production. On the other hand, considering that nanostructured catalysts in the form of film will display better durability and reusability, the Ti-supported $NiCo_2O_4$ nanosheet array rather than $NiCo_2O_4$ nanostructures in the form of powder is designed in the present study. Considering its low cost, high mechanical strength, together with its high stability in different chemical environments, Ti is selected as the substrate in our work. It is interesting to find that the turnover frequency (TOF) of $NiCo_2O_4$/Ti in AB hydrolysis can reach 50.1 mol H_2 min^{-1} (mol catalyst)$^{-1}$. To the best of our knowledge, this is the highest TOF value reported in the literature for noble-metal-free catalysts towards AB hydrolysis. In addition, the Ti-supported $NiCo_2O_4$ nanosheet array exhibits significantly improved durability and reusability compared with those nanocatalysts recently reported in the literature, which enable it to be a strong catalyst candidate in AB hydrolysis for the generation of hydrogen for practical applications.

Experimental section

Synthesis

All reagents were of analytical grade and used as received without further purification. Double-distilled water was used throughout the experiments. To prepare the $NiCo_2O_4$ nanosheet array supported on Ti substrate, 4.0 mmol of $CoCl_2{\cdot}6H_2O$ and 2.0 mmol $NiCl_2{\cdot}6H_2O$ was mixed into 20.0 mL of double-distilled water under stirring to form solution A, and 12.0 mmol sodium citrate was dissolved into 20.0 mL of water to form solution B. After solution A and B were blended, 40.0 mL of NaOH (7.5 M) solution were dropped into the above solution. Afterwards, the mixed solution was quickly transferred into a Teflon-lined steel autoclave, in which a piece of 5 × 12 cm Ti sheet with a thickness of *ca.* 20 μm and a weight of *ca.* 0.72 g (purchased from Qingyuan Metallic materials Co., Ltd., China) closely attached to the inner wall of the vessel was used as support. Finally, the autoclave was kept in an air oven at 160 °C for 10 h. After that, the sample was transferred into a muffle furnace and subjected to a heat treatment at 400 °C for 4 h. After the reaction, the film was taken out and washed with double-distilled water and acetone, then dried in a vacuum oven at 60 °C for 5 h. For comparison, the $NiCo_2O_4$ nanoparticles were also prepared by a similar process except that no Ti substrate was used in the synthesis. Briefly, $CoCl_2{\cdot}6H_2O$, $NiCl_2{\cdot}6H_2O$ and sodium citrate at a molar ratio of 2 : 1 : 6 were mixed into water under intense stirring to form a mixed solution. After the addition of the NaOH solution, the mixed solution was subjected to a hydrothermal treatment at 160 °C for 10 h. Then, the collected black powder was heated at 400 °C for 4 h.

Characterization

X-ray diffraction (XRD) patterns were recorded using a PANalytical B. V. Empyean X-ray diffractometer with Cu Kα radiation (λ = 1.5406 Å). The morphology of the array was investigated using a Hitachi S-4800 field emission scanning electron microscope (FE-SEM). TEM images were obtained on a Tecnai G2 F20 S-TWINT transmission electron microscope. X-ray photoelectron spectra (XPS) were obtained on a VG ESCALAB 210 X-ray photoelectron spectrometer with Al Kα radiation. The specific surface area was measured on a Quantachrome Autosorb-1 volumertic analyzer, using nitrogen adsorption and the Brunauer–Emmett–Teller method. The weight of $NiCo_2O_4$ loaded on the Ti substrate was measured by a Varian 720 Inductively Coupled Plasma-Optical Emission Spectrometer (ICP-OES).

Catalytic performance testing

The catalytic performance of the $NiCo_2O_4$/Ti and $NiCo_2O_4$ nanoparticles were assessed by measuring the accumulative volume of hydrogen generated during the AB hydrolysis reaction in a glass reactor connected with a gas burette. Typically, 20.0 mL of freshly-prepared mixed solution of AB (0.15 M) and NaOH (1 M) was added in the reactor. Then, the $NiCo_2O_4$/Ti (5 cm × 3 cm) was added into the AB solution. The reaction temperature was maintained at 308 ± 0.5 K in a thermostated reactor. The reusability of the $NiCo_2O_4$/Ti was evaluated by repeating the hydrolysis reaction 10 times in such a model: (1) recollecting the catalyst after the reaction; (2) washing the catalyst with water and ethanol alternately before drying at 50 °C in a vacuum oven; and (3) starting a new run of AB hydrolysis by mixing the catalyst with freshly-prepared AB solution.

Results and discussion

The digital camera photos of the bare Ti sheet and $NiCo_2O_4$/Ti are presented in Fig. S1 (see the ESI†). As can be seen, the bare Ti substrate is silver gray with metallic luster (Fig. S1a†) while $NiCo_2O_4$/Ti is black (Fig. S1b†), implying that the black $NiCo_2O_4$ has been successfully deposited on the Ti sheet in this study. The microstructures on the surface of the Ti substrate and $NiCo_2O_4$/Ti are investigated by FE-SEM. As can be observed in Fig. 1, the Ti substrate is very smooth on its surface (Fig. 1a). In contrast, it became very coarse after the deposition of $NiCo_2O_4$ (Fig. 1b). Fig. 1c reveals that the $NiCo_2O_4$ layer on the substrate is comprised of the $NiCo_2O_4$ nanosheet array, which looks somewhat like flowers. Fig. 1d indicated that the mean thickness of the nanosheets is about 20 nm. Obviously, these nanosheets are not loosely agglomerated but

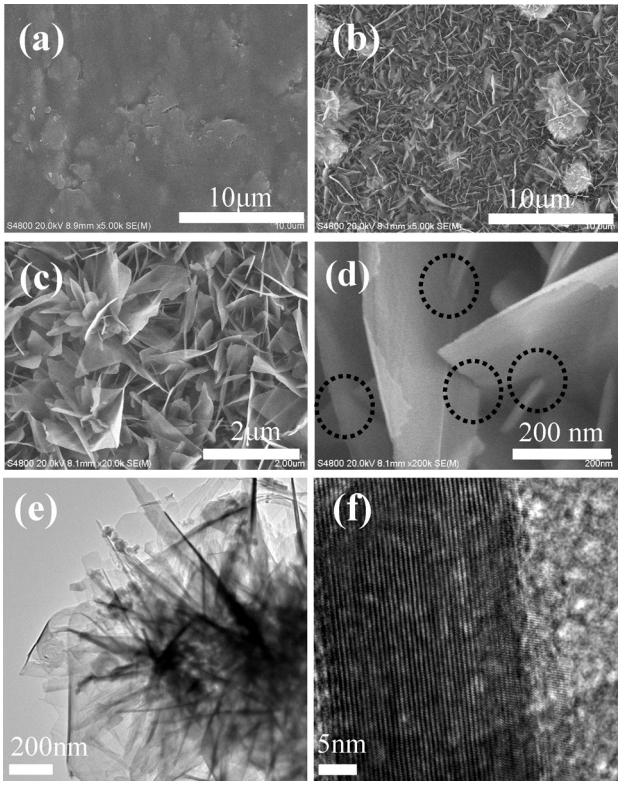

Fig. 1 SEM images of the bare Ti substrate (a) and $NiCo_2O_4$/Ti (b–d). TEM image of the $NiCo_2O_4$ nanosheet array (e) and cross-section TEM image of a piece of $NiCo_2O_4$ nanosheet (f).

closely interconnected to each other, which is marked with the dotted circles in Fig. 1d. It is worth noting that an ultrasonic treatment of 30 min cannot detach these $NiCo_2O_4$ nanosheets from the Ti substrate, hinting that the as-prepared $NiCo_2O_4$ nanosheet array is very stable. Besides, a peeling test using scotch tape was also carried out (experiment details about the peeling test can be seen in the ESI†), and it was found that no $NiCo_2O_4$ was detached from the substrate after the test. This further demonstrates the good stability of our sample. Fig. 1e shows the TEM image of the $NiCo_2O_4$ nanosheet array, which further confirms the nanostructures of the $NiCo_2O_4$ nanosheets. Fig. 1f shows the cross-section TEM image of a piece of $NiCo_2O_4$ nanosheet, demonstrating a thickness of *ca.* 20 nm. The ICP-OES analysis indicates that the weight of $NiCo_2O_4$ loaded on the Ti sheet (5 × 12 cm) is *ca.* 9.6 mg.

The crystal structures of the Ti sheet-supported $NiCo_2O_4$, as well as the Ti substrate, were investigated by XRD. As depicted in Fig. 2, seven characteristic peaks at 2θ = 35.2°, 38.4°, 40.3°, 53.0°, 63.0°, 70.6° and 76.2° are observed in the XRD pattern of the Ti substrate, which can be indexed to the (100), (002), (101), (102), (110), (103) and (112) plane reflections of the hexagonal close-packed phase of Ti (PDF#65-9622). Besides these seven peaks, eight characteristic peaks appear in the XRD pattern of $NiCo_2O_4$/Ti, which can be assigned to the diffractions from (220), (311), (400), (331), (442), (511), (440) and (533) planes of the cubic phase of

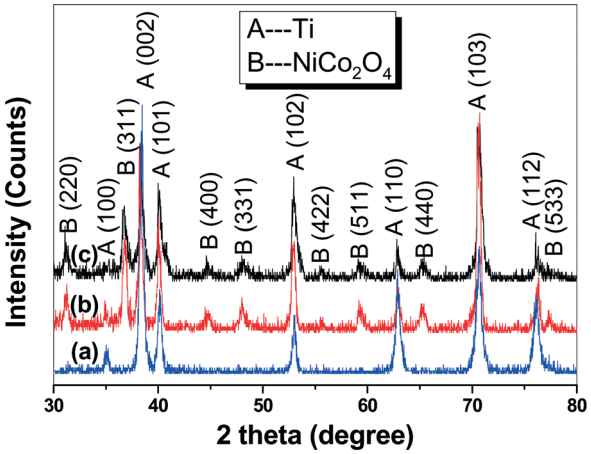

Fig. 2 XRD patterns of the bare Ti substrate (a), the as-prepared $NiCo_2O_4$/Ti (b) and the $NiCo_2O_4$/Ti after 10 catalytic cycles (c).

$NiCo_2O_4$ (PDF#73-1702). This result further confirms that the $NiCo_2O_4$ has been successfully deposited on the Ti substrate.

To obtain the information about the chemical states of Co and Ni in $NiCo_2O_4$/Ti, XPS analysis was carried out. As

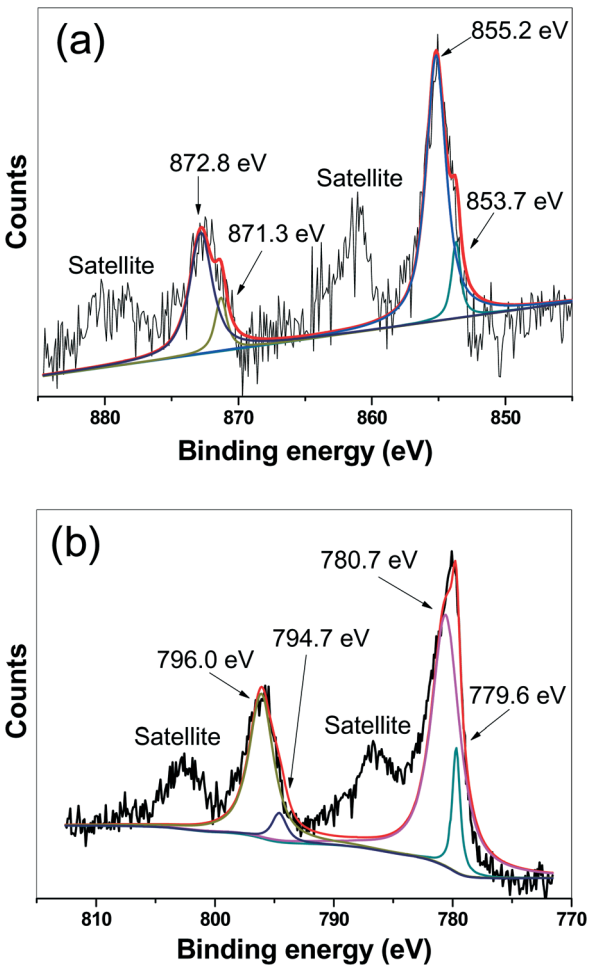

Fig. 3 XPS spectra of $NiCo_2O_4$/Ti in the regions of Ni 2p (a) and Co 2p (b).

displayed in Fig. 3, the deconvoluted XPS spectrum shows two peaks at the binding energies of *ca.* 872.8 and 871.3 eV in the region of Ni $2p_{1/2}$, and two peaks at the binding energies of *ca.* 855.2 and 853.7 eV in the region of Ni $2p_{3/2}$. The peaks at the binding energies of *ca.* 872.8 and 855.2 eV can be indexed to Ni(III), while those at the binding energies of *ca.* 871.3 and 853.7 can be assigned to Ni(II).[26] Similarly, the deconvoluted XPS spectrum shows two peaks at the binding energies of *ca.* 796.0 and 794.7 eV in the region of Co $2p_{1/2}$, and two peaks at the binding energies of *ca.* 780.7 and 779.6 eV in the region of Co $2p_{3/2}$. The peaks at the binding energies of *ca.* 779.6 eV and 794.6 eV can be indexed to Co(III), while those at the binding energies of *ca.* 780.7 eV and 796.0 eV can be assigned to Co(II).[26] XPS analysis reveals that Co^{2+}, Co^{3+}, Ni^{2+} and Ni^{3+} coexist on the surface of the $NiCo_2O_4$/Ti sample, which is similar to the XPS results of the $NiCo_2O_4$ nanostructures reported by other groups.[24,26,27]

The release of hydrogen from the AB solution catalyzed by the as-prepared $NiCo_2O_4$/Ti was investigated. First, the catalytic activity of the Ti substrate in the AB hydrolysis is checked. It was found that nearly no hydrogen is produced from the AB solution when the bare Ti sheet is presented in the reaction system, demonstrating that the Ti substrate is inactive towards AB hydrolysis. When $NiCo_2O_4$/Ti is added into the AB solution, a certain amount of hydrogen will be generated, suggesting that the $NiCo_2O_4$ on the Ti substrate can catalyze the AB hydrolysis. Fig. 4a shows the accumulated volume of hydrogen *vs.* the hydrolysis time at catalyst dosages ranging from 0.3 to 3.6 mg. It is observed that the accumulated hydrogen volume is almost directly proportional to the reaction time at the early stage of the hydrolysis, hinting that the hydrolysis process follows the zero-order kinetics with respect to ammonia borane. To confirm this, a series of catalytic hydrolysis experiments with different initial concentrations of AB were carried out and the results are shown in Fig. S2 in the ESI.† As can be seen in Fig. S2,† the rate constants almost remain the same despite the fact that the initial concentrations of AB in the catalytic process are different, demonstrating that the hydrolysis process follows the zero-order kinetics with respect to AB. Note that a deviation from the linear dependence of the accumulated hydrogen volume with the reaction time was observed at the late stage of the hydrolysis reaction, which may result from the external diffusion limitation at a low concentration of AB.[7] The rate constant of AB hydrolysis can be determined from the linear portion of each plot, which can be formulated as follows:

$$k = V/t$$

where k, V, t are the rate constant, accumulated volume of hydrogen and hydrolysis time, respectively. Fig. 4b depicts the effect of catalyst dosage on the rate constants. Clearly, k increases linearly with the mass of $NiCo_2O_4$. This implies that the hydrogen production rate can be easily controlled by adjusting the amount of $NiCo_2O_4$ catalysts. It should be mentioned that this is the first investigation into the catalytic

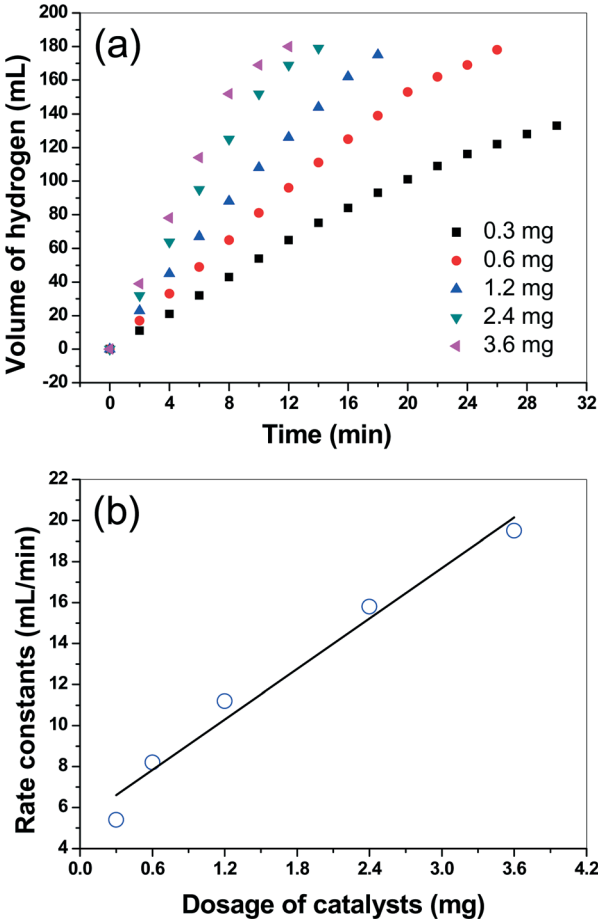

Fig. 4 (a) The accumulated volume of generated hydrogen *vs.* reaction time at different catalyst dosages; (b) the rate constants at different catalyst dosages.

hydrolysis of AB catalyzed by $NiCo_2O_4$ and the kinetics data on it is unavailable in the literature. For comparison, $NiCo_2O_4$ particles with a typical diameter of 15–25 nm were prepared and the SEM images are shown in Fig. S3 (see the ESI†). A series of contrast experiments were carried out, in which the $NiCo_2O_4$ nanoparticles instead of $NiCo_2O_4$/Ti acted as catalysts. The rate constants of AB hydrolysis in the presence of the $NiCo_2O_4$ nanoparticles and the $NiCo_2O_4$/Ti as catalysts were compared and the results are indicated in Table 1. It is interesting to note that the rate constants of AB hydrolysis for the $NiCo_2O_4$/Ti catalyst are 10–12 times as large as those for the $NiCo_2O_4$ nanoparticles although the BET surface area of $NiCo_2O_4$/Ti is only *ca.* 1.4 times as large as that of the $NiCo_2O_4$ nanoparticles. Two factors account for the fact that the $NiCo_2O_4$/Ti catalyst exhibits better catalytic performance in contrast to the $NiCo_2O_4$ nanoparticles. First, the $NiCo_2O_4$ layer in the $NiCo_2O_4$/Ti catalysts are composed of nanosheets, which are expected to possess more corners and edges compared with the spherical $NiCo_2O_4$ nanoparticles. In general, the atoms on the corners or edges have unsaturated valency with lower number of bonds around them compared with those in the interiors or on the faces.[28,29] Thus, such atoms will display much higher intrinsic catalytic activity.

Table 1 The BET surface of the $NiCo_2O_4$/Ti and $NiCo_2O_4$ nanoparticles, and the comparison of rate constants of AB hydrolysis catalyzed by $NiCo_2O_4$/Ti and $NiCo_2O_4$ nanoparticles at different dosages

Sample	Rate constant (min^{-1})					BET surface ($m^2\ g^{-1}$)
	0.3 mg	0.6 mg	1.2 mg	2.4 mg	3.6 mg	
$NiCo_2O_4$/Ti	5.4	8.2	11.2	15.8	19.5	65.5[a]
$NiCo_2O_4$ nanoparticles	0.51	0.77	1.03	1.36	1.61	47.2

[a] The mass in the BET surface of $NiCo_2O_4$/Ti only counts the mass of $NiCo_2O_4$, not including that of Ti substrate.

Second, the $NiCo_2O_4$ nanoparticles suspended in the AB solution tend to aggregate on account of the high surface energy. Under such circumstances, the number of active sites of particulate $NiCo_2O_4$ will drop, which will result in the decrease of their catalytic activity. On the contrary, the $NiCo_2O_4$ nanosheets in the $NiCo_2O_4$/Ti catalyst are immobilized on the Ti sheet. In this case, the decline of catalytic performance which resulted from the aggregation is inevitable.

In this study, AB hydrolysis catalyzed by the $NiCo_2O_4$/Ti catalyst was carried out at different reaction temperatures and the relationship between the volumes of hydrogen and the reaction time is displayed in Fig. 5a. It is found that elevating the reaction temperature from 298 K to 308 K will cause a pronounced increase in the hydrolysis rate of AB. While a further elevation of temperature to 318 K and 328 K only results in a slight increase of hydrolysis rate of AB. The corresponding TOF value of the $NiCo_2O_4$/Ti sample at 298 K is figured out to be *ca.* 50.1 mol H_2 min^{-1} (mol catalyst)$^{-1}$. For comparison, the TOF values of some noble-metal-based and noble-metal-free nanocatalysts recently reported in the literature are also listed in Table 2. Evidently, our $NiCo_2O_4$/Ti catalyst falls into the class of high-performance catalysts towards AB hydrolysis. To the best of our knowledge, among the noble-metal-free heterogeneous catalysts for AB hydrolysis, the $NiCo_2O_4$/Ti catalyst exhibits the highest catalytic activity in terms of TOF.

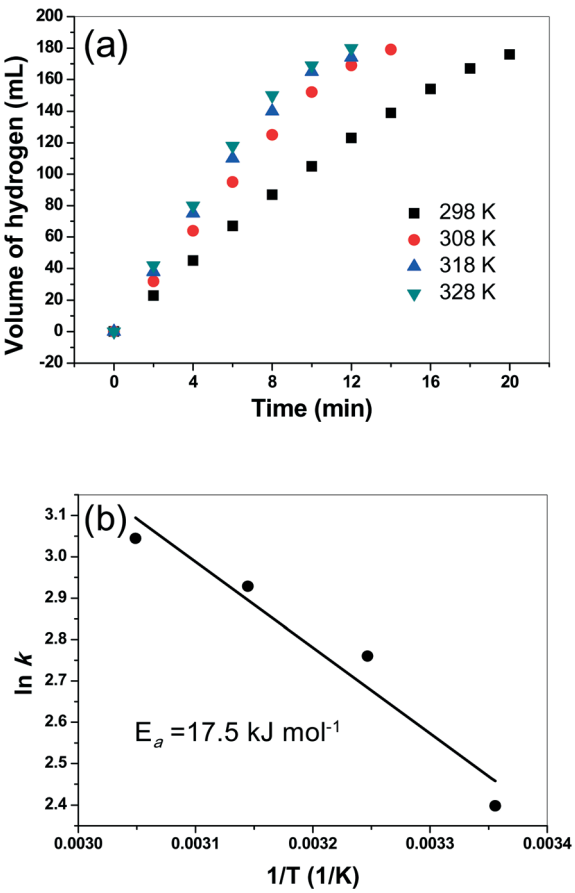

Fig. 5 (a) The accumulated volume of generated hydrogen *vs.* reaction time at different reaction temperatures; (b) the logarithm of rate constants *vs.* the reciprocal of reaction temperatures; catalyst dosage = 2.4 mg.

The apparent activation energy (E_a) is an important parameter for a catalytic reaction, which can be utilized to assess the overall catalytic activity of a catalyst. Generally, a catalyst with higher catalytic activity always leads to lower activation energy of the catalytic reaction. According to the Arrhenius formula, the apparent activation energy of AB hydrolysis catalyzed by the $NiCo_2O_4$/Ti catalyst can be figured out based on the data on rate constants at different temperatures. Fig. 5b displays the logarithm of the rate constants *vs.* the reciprocal of the corresponding reaction temperatures. According to the slope of the fitted line in Fig. 5b, the E_a value for AB hydrolysis catalyzed by the $NiCo_2O_4$/Ti catalyst was calculated to be 17.5 kJ mol^{-1}. This value is even much lower than the E_a value for AB hydrolysis catalyzed by noble-metal-based nanocatalysts (Table 2), hinting at the superior catalytic activity of the $NiCo_2O_4$/Ti catalyst.

In addition to the activity, the recyclability of a heterogeneous catalyst is of great importance in practical applications. In the present study, the hydrolysis of AB catalyzed by the $NiCo_2O_4$/Ti catalyst was repeated 10 times. The relationship between the accumulated volume of generated hydrogen and reaction time at different cycles is shown in Fig. S4.† The normalized rate constant, *viz.* k_n/k_1, where k_1 and k_n severally denotes the rate constant of AB hydrolysis in cycles No. 1 and No. n, is utilized to assess the durability and reusability of the $NiCo_2O_4$/Ti catalyst. As displayed in Fig. 6, the hydrolysis efficiency decreases marginally from 96% at the first cycle to 92% at the 10th cycle. As for the rate constant of AB hydrolysis, it almost remains unchanged in the first 6 cycles and decreases slightly in the following cycles. At the 10th cycle, the normalized rate constant is *ca.* 0.9, indicating that the $NiCo_2O_4$/Ti catalyst still retains 90% of its original activity. Our $NiCo_2O_4$/Ti catalyst exhibits much improved durability

Table 2 Comparison of TOF and E_a of different catalysts in AB hydrolysis

Catalysts	TOF (mol H_2 min^{-1} (mol cat.)$^{-1}$)	E_a (kJ mol^{-1})	Ref.
Pt cube/CeO_2/RGO	48.0	—	30
Pt NPs/CeO_2/RGO	30.6	—	30
Ru@Al_2O_3	39.6	48	31
Ru nanoparticles	21.8	27.5	10
Ru/graphene	100	11.7	32
Pd-CDG	15.5	—	33
Pd(0)–HAP	8.3	55	34
RuCu/graphene	135	30.59	35
PtPt nanocubes	50.0	21.8	36
Pt–Pd@PVP	125	51.7	15
$Ni_{30}Pd_{70}$/RGO	28.7	45	14
Pd@Co/graphene	37.5	—	37
$Co_{35}Pd_{65}$/C	22.7	27.5	12
Ag–Pd/PAN	6.3	—	38
Co/graphene	13.8	32.75	39
Co–P/TiO_2	5.3	48.1	40
Electroplated Co–P	10.0	22	21
CoNi/graphene	16.4	13.49	41
Ni nanoparticles	10.9	—	42
Nanoporous Ni spheres	19.6	27	43
Ni NPs@3D GFs	41.7	—	19
Co film	6.6	59	16
Co–B film	21.6	34	20
$NiCo_2O_4$	50.1	17.5	This work

The TOF values were either directly taken or calculated from the data given in respective references.

and reusability in contrast to recently reported nanocatalysts, such as Co–graphene (40% activity loss after 5 cycles[39]), CoNi@graphene (56% activity loss after 5 cycles[41]), Pd–Pt@PVP (39% activity loss after 5 cycles[15]), Pt/RGO (54% activity loss after 5 cycles[30]), Ru/g-C_3N_4 (50% activity loss after 4 cycles[44]), Co film (40% activity loss after 6 cycles[16]), and intrazeolite Co(0) nanoclusters (31% activity loss after 5 cycles[18]).

For those nanocatalysts in the form of powder, the material loss during the process of separation, drying and re-

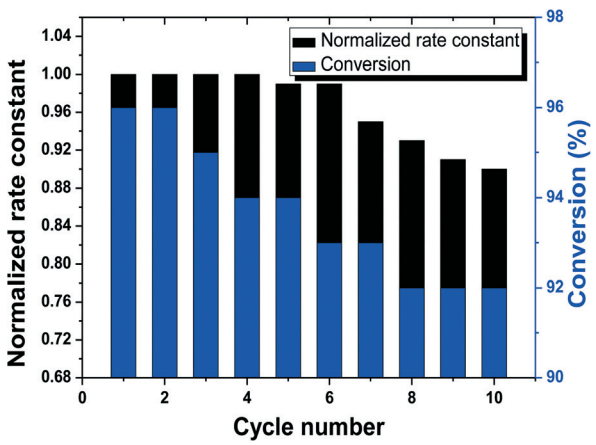

Fig. 6 Normalized rate constants and conversion at different cycles (catalyst dosage = 2.4 mg).

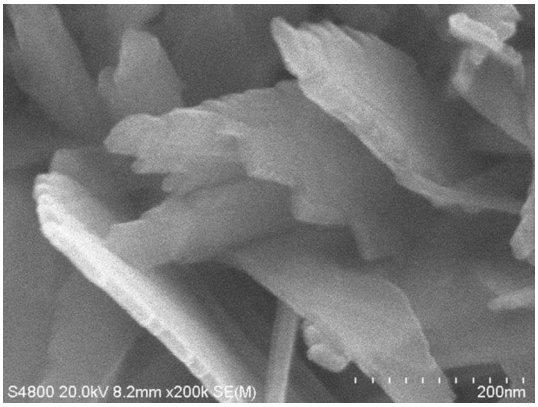

Fig. 7 High-magnification SEM image of $NiCo_2O_4$/Ti after 10 cycles (catalyst dosage = 2.4 mg).

dispersion will cause the drop of the activity of the catalysts.[18] Also, under the drive of high surface energy, the fine powdery particles are very likely to aggregate during the process of usage, isolation and desiccation, which will result in a remarkable loss of the catalytic activity in the long-term run. In contrast, the $NiCo_2O_4$ nanosheets in the array are immobilized on the Ti substrate. So, they are exempt from the activity drop caused by the migration and aggregation of the $NiCo_2O_4$ nanosheets. Besides, the alteration of shapes and morphology of the nanocatalysts during the catalytic process can also influence their catalytic performance.[29] To clarify this, the SEM image of $NiCo_2O_4$/Ti after 10 cycles of catalytic reaction is shown in Fig. 7, demonstrating that there were no remarkable morphology changes in the $NiCo_2O_4$/Ti catalyst. Also, the XRD pattern of $NiCo_2O_4$/Ti after 10 cycles is similar to that of the fresh $NiCo_2O_4$/Ti. These observations hint that our $NiCo_2O_4$/Ti catalyst is stable and reusable in the reaction of AB hydrolysis.

Conclusions

In summary, the array of $NiCo_2O_4$ nanosheets with a thickness of about 20 nm supported on Ti substrate ($NiCo_2O_4$/Ti) was successfully prepared. It has been demonstrated that the as-prepared $NiCo_2O_4$/Ti catalyst exhibits high catalytic performance in the hydrolysis of AB for hydrogen production. The TOF value of $NiCo_2O_4$/Ti is 50.1 mol H_2 min^{-1} (mol catalyst)$^{-1}$. To the best of our knowledge, this value is higher than those of the other noble-metal-free catalysts in the literature. The apparent activation energy of AB hydrolysis in the presence of the $NiCo_2O_4$/Ti catalyst is as low as *ca.* 17.5 kJ mol^{-1}. More importantly, the $NiCo_2O_4$/Ti catalyst still maintains about 90% of its original catalytic activity after 10 cycles, exhibiting significantly improved durability and the reusability compared with many other nanocatalysts reported in the literature. Its high catalytic activity and low-cost, together with its good durability and reusability enable $NiCo_2O_4$/Ti to be a strong catalyst candidate towards the AB hydrolysis for hydrogen generation in practical applications.

Acknowledgements

This work was financially supported by the National Natural Science Foundation of China (No. 51001052), the Natural Science Foundation of Guangdong Province (No. S2013010015681), the High-level Talent Project of the University in Guangdong Province (184), the Characteristic and Innovative Project of the Education Department of Guangdong Province (No. 2014KTSCX177) and the Foundation for Distinguished Young teachers in Higher Education of Guangdong (No. Yq2013154).

Notes and references

1 J. A. Turner, *Science*, 2004, **305**, 972.
2 V. I. Simagina, P. A. Storozhenko, O. V. Netskina, O. V. Komova, G. V. Odegova, Y. V. Larichev, A. V. Ishchenko and A. M. Ozerova, *Catal. Today*, 2008, **138**, 253.
3 H. Li, J. Liao, X. Zhang, W. Liao, L. Wen, J. Yang, H. Wang and R. Wang, *J. Power Sources*, 2013, **239**, 277.
4 G. H. Liu and Z. P. Li, *J. Power Sources*, 2009, **187**, 527.
5 W. Chen, J. Ji, X. Duan, G. Qiang, P. Li, X. Zhou and D. Chen, *Chem. Commun.*, 2014, **50**, 2142.
6 L. He, Y. Huang, X. Y. Liu, L. Li, A. Wang, X. Wang, C. Y. Mou and T. Zhang, *Appl. Catal., B*, 2014, **147**, 779.
7 W. Chen, J. Ji, X. Feng, X. Duan, G. Qian, P. Li, X. Zhou, D. Chen and W. Yuan, *J. Am. Chem. Soc.*, 2014, **136**, 16736.
8 S. Basu, A. Brockman, P. Gagare, Y. Zheng, P. Ramachandran, W. Delgass and J. Gore, *J. Power Sources*, 2009, **188**, 238.
9 S. Akbayrak and S. Özkar, *Dalton Trans.*, 2014, **43**, 1797.
10 E. K. Abo-Hamed, T. Pennycook, Y. Vaynzof, C. Toprakcioglu, A. Koutsioubas and O. A. Scherman, *Small*, 2014, **10**, 3145.
11 S. Akbayrak, M. Kaya, M. Volkan and S. Özkar, *Appl. Catal., B*, 2014, **147**, 387.
12 D. Sun, V. Mazumder, Ö. Metin and S. Sun, *ACS Nano*, 2011, **5**, 6458.
13 K. Güngörmez and Ö. Metin, *Appl. Catal., A*, 2015, **494**, 22.
14 N. S. Ciftci and Ö. Metin, *Int. J. Hydrogen Energy*, 2014, **39**, 18863.
15 M. Rakap, *J. Power Sources*, 2015, **276**, 320.
16 M. Paladini, G. M. Arzac, V. Godinho, M. C. Jiménez De Haro and A. Fernández, *Appl. Catal., B*, 2014, **158**, 400.
17 J. Liao, H. Li and X. Zhang, *Catal. Commun.*, 2015, **67**, 1.
18 M. Rakap and S. Özkar, *Int. J. Hydrogen Energy*, 2010, **35**, 3341.
19 M. Mahyari and A. Shaabani, *J. Mater. Chem. A*, 2014, **2**, 16652.
20 N. Patel, R. Fernandes, G. Guella and A. Miotello, *Appl. Catal., B*, 2010, **95**, 137.
21 K. S. Eom, K. W. Cho and H. S. Kwon, *Int. J. Hydrogen Energy*, 2010, **35**, 181.
22 R. Fernandes, N. Patel, A. Miotello and L. Calliari, *Top. Catal.*, 2012, **55**, 1032.
23 W. Liu, C. Lu, K. Liang and B. K. Tay, *J. Mater. Chem. A*, 2014, **2**, 5100.
24 C. Yuan, J. Li, L. Hou, X. Zhang, L. Shen and X. W. Lou, *Adv. Funct. Mater.*, 2012, **22**, 4592.
25 G. Q. Zhang, H. B. Wu, H. E. Hoster, M. B. Chan-Park and X. W. Lou, *Energy Environ. Sci.*, 2012, **5**, 9453.
26 C. Yuan, J. Li, L. Hou, L. Yang, L. Shen and X. Zhang, *J. Mater. Chem.*, 2012, **22**, 16084.
27 R. Zou, K. Xu, T. Wang, G. He, Q. Liu, X. Liu, Z. Zhang and J. Hu, *J. Mater. Chem. A*, 2013, **1**, 8560.
28 M. A. Mahmoud, F. Saira and M. A. El-Sayed, *Nano Lett.*, 2010, **10**, 3764.
29 X. Liu, D. Wang and Y. Li, *Nano Today*, 2012, **7**, 448.
30 X. Wang, D. Liu, S. Song and H. J. Zhang, *Chem. - Eur. J.*, 2013, **19**, 8082.
31 H. Can and Ö. Metin, *Appl. Catal., B*, 2012, **125**, 304.
32 N. Cao, W. Luo and G. Z. Cheng, *Int. J. Hydrogen Energy*, 2013, **38**, 11964.
33 Ö. Metin, E. Kayhan, S. Özkar and J. J. Schneider, *Int. J. Hydrogen Energy*, 2012, **37**, 8161.
34 M. Rakap and S. Özkar, *Int. J. Hydrogen Energy*, 2011, **36**, 7019.
35 N. Cao, K. Hu, W. Luo and G. Cheng, *J. Alloys Compd.*, 2014, **590**, 241.
36 A. J. Amali, K. Aranishi, T. Uchida and Q. Xu, *Part. Part. Syst. Charact.*, 2013, **30**, 888.
37 J. Wang, Y. L. Qin, X. Liu and X. B. Zhang, *J. Mater. Chem.*, 2012, **22**, 12468.
38 Y. Tong, X. Lu, W. Sun, G. Nie, L. Yang and C. Wang, *J. Power Sources*, 2014, **261**, 221.
39 L. Yang, N. Cao, C. Du, H. Dai, K. Hu, W. Luo and G. Cheng, *Mater. Lett.*, 2014, **115**, 113.
40 M. Rakap, *J. Power Sources*, 2014, **265**, 50.
41 W. Feng, L. Yang, N. Cao, C. Du, H. Dai, W. Luo and G. Cheng, *Int. J. Hydrogen Energy*, 2014, **39**, 3371.
42 J. M. Yan, X. B. Zhang, S. Han, H. Shioyama and Q. Xu, *Inorg. Chem.*, 2009, **48**, 7389.
43 C. Y. Cao, C. Q. Chen, W. Li, W. G. Song and W. Cai, *ChemSusChem*, 2010, **3**, 1241.
44 Y. Fan, X. Li, X. He, C. Zeng, G. Fan, Q. Liu and D. Tang, *Int. J. Hydrogen Energy*, 2014, **39**, 19982.